Computational and experimental study of gas flows through long channels of various cross sections in the whole range of the Knudsen number

Stelios Varoutis and Steryios Naris
Department of Mechanical and Industrial Engineering, University Thessaly, Volos 38334, Greece

Volker Hauer and Christian Day
Institute of Technical Physics, Forschungszentrum Karisruhe, Karlsruhe 76021, Germany

Dimitris Valougeorgis[a)]
Department of Mechanical and Industrial Engineering, University Thessaly, Volos 38334, Greece

(Received 15 August 2008; accepted 10 November 2008; published 30 December 2008)

A computational and experimental study has been performed for the investigation of fully developed rarefied gas flows through channels of circular, orthogonal, triangular, and trapezoidal cross sections. The theoretical-computational approach is based on the solution of the Bhatnagar-Gross-Krook kinetic equation subject to Maxwell diffuse-specular boundary conditions by the discrete velocity method. The experimental work has been performed at the vacuum facility "TRANSFLOW," at Forschungszentrum Karlsruhe and it is based on measuring, for assigned flow rates, the corresponding pressure differences. The computed and measured mass flow rates and conductance are in all cases in very good agreement. In addition, in order to obtain some insight in the flow characteristics, the reference Knudsen, Reynolds, and Mach numbers characterizing the flow at each experimental run have been estimated. Also, the pressure distribution along the channel for several typical cases is presented. Both computational and experimental results cover the whole range of the Knudsen number. © *2009 American Vacuum Society.* [DOI: 10.1116/1.3043463]

I. INTRODUCTION

The investigation of rarefied gas flows in channels of various cross sections is of major theoretical and practical importance. The degree of rarefaction is specified by the estimation of the Knudsen number, which is defined as the ratio of the mean free path to a characteristic length scale. In general, there are four regimes: the continuum or viscous regime, the slip regime, the transition or Knudsen regime, and the free molecular regime.[1,2] The computational and experimental results presented here refer to flows through channels of circular, orthogonal, triangular, and trapezoidal cross sections and cover all four regimes.

Applications of such flows may be found in several engineering fields including nano- and microfluidics, high altitude gas dynamics, aerosol industry, porous media, and vacuum technology. The latter one is one of the most significant applications of rarefied gas flows and the motivation for the present study. In several vacuum applications, such as the vacuum systems of fusion reactors, the flow may be under rough, medium, and high (or ultrahigh) vacuum conditions. Therefore, the flow may be in the whole range of the Knudsen number from the free molecular through the transition and slip regimes up to the hydrodynamic limit.

Rarefied gas flows may be treated theoretically with several methodologies.[3–6] For fully developed flows, as the ones considered in the present work, the most powerful approach is, by far, the kinetic theory approach.[3,7] In this case, kinetic-type formulations, based on the Boltzmann equation or on simplified kinetic model equations, may take advantage of all flow characteristics and properties and yield a set of simple linearized kinetic model equations, which are solved in a very accurate and computationally efficient manner. Rarefied gas flows in long circular channels have been investigated via kinetic theory from the 1960s, implementing semianalytical and numerical schemes. An extended and profound review for linearized flows in circular channels is given in Ref. 8.

The extension of all these schemes to flows through channels of noncircular cross sections is not trivial or straightforward since now the flow is not axisymmetric. Results for flows through channels of various cross sections, based on the integromoment method, have been presented in Refs. 9 and 10 and also in the review article.[11] More recently, the discrete velocity method has been applied to solve flows through channels of rectangular,[12,13] ellipsoidal,[14] circular annulus,[15] and triangular[16] cross sections in a very accurate and computationally efficient manner. It is noted that no results have been reported so far for flows through channels of trapezoidal cross sections, which are common in the vacuum pumping systems of fusion reactors as well as in microchannels fabricated by silicon wet etching.

Rarefied gas flows through long channels have been also investigated experimentally. Early work has been performed in vacuum systems measuring the conductance in circular channels[17–19] and more recently in capillaries.[20,21] During the last decade, this effort has been extended to microsystems, where extensive experimental measurements have been performed mainly with orthogonal microchannels.[22–27] However, most experimental results are for small up to moderate

[a)]Author to whom correspondence should be addressed; electronic mail: diva@mie.uth.gr

Knudsen numbers. Also, the authors are not aware of any experimental work in triangular and trapezoidal cross sections.

In the present work we study fully developed flows through channels of various cross sections, including triangular and trapezoidal ones. The investigation is both computational and experimental, and the main objective is the comparison between computed and measured quantities of the mass flow rate and the conductance. In addition, several flow characteristics and properties are presented and discussed in detail. The results cover the whole range of the Knudsen number.

In Sec. II, the flow configuration is described and the basic dimensionless quantities are defined. In Sec. III, the formulation of the problem is presented in a unified manner for all cross sections to allow a direct comparison with the experimental results. The experimental test rigs including the calibration and measurement procedures are described in Sec. IV. Computational and experimental results are presented and discussed in Sec. V, while some closing remarks are given in Sec. VI.

II. FLOW CONFIGURATION

The flow configuration presented in this section is general and applies to channels of any cross section including the four cross sections under consideration. Consider the isothermal flow of a gas at a reference temperature T_0 through a long channel of length L and hydraulic diameter D_h, connecting two reservoirs maintained at pressures P_1 and P_2, respectively, with $P_1 > P_2$. The area and the perimeter of the cross section are denoted by $\tilde{A}$ and $\tilde{\Gamma}$, respectively, while the reference pressure is defined as $P_0=(P_1+P_2)/2$. By taking $D_h \ll L$ the flow is considered as fully developed, and then, end effects at the inlet and the outlet of the channel are ignored. Even more, at each cross section the pressure is constant and varies only along the flow direction $\tilde{z}$, i.e., $P=P(\tilde{z}) \in [P_1, P_2]$. The flow is driven by the imposed dimensionless pressure gradient

$$X_P = \frac{D_h}{P}\frac{dP}{d\tilde{z}}, \tag{1}$$

where

$$D_h = \frac{4\tilde{A}}{\tilde{\Gamma}}. \tag{2}$$

The only nonzero component of the macroscopic (bulk) velocity is the one in the $\tilde{z}$ direction and it is denoted by $\tilde{u}(\tilde{x},\tilde{y})$, where $\tilde{x}$ and $\tilde{y}$ are the lateral coordinates.

The basic parameter of the flow is the Knudsen number defined by[8]

$$\mathrm{Kn} = \frac{\sqrt{\pi}}{2}\frac{\mu_0 \upsilon_0}{D_h P}, \tag{3}$$

where μ_0 is the gas viscosity at temperature T_0 and $\upsilon_0 = \sqrt{2RT_0}$, with $R=k/m$ denoting the gas constant (k is the Boltzmann constant and m the molecular mass), is the most probable molecular velocity. It is noted that in Ref. 8 the Knudsen number is defined in terms of the radius of the tube, while here, since channels of various cross sections are considered, it is defined in terms of the hydraulic diameter of the cross section. In addition to the Knudsen number the other two characteristic and commonly used numbers of the flow are the Reynolds and Mach numbers defined as

$$\mathrm{Re} = \frac{\rho \tilde{U} D_h}{\mu_0} \tag{4}$$

and

$$\mathrm{Ma} = \frac{\tilde{U}}{c_0}, \tag{5}$$

respectively. Here, ρ is the mass density ($P=\rho RT_0$), $c_0 = \upsilon_0\sqrt{\gamma/2}$ is the adiabatic sound velocity at temperature T_0, and γ is the specific heat ($\gamma=5/3$ for a monoatomic gas), while

$$\bar{U} = \frac{1}{\tilde{A}}\int_{\tilde{A}} \bar{u}(\bar{x},\bar{y})\, d\tilde{A} \tag{6}$$

is the mean macroscopic velocity. Based on Eqs. (3)–(5) it is readily seen that[25]

$$\mathrm{Kn} = \sqrt{\frac{\pi}{2}}\sqrt{\gamma}\frac{\mathrm{Ma}}{\mathrm{Re}}. \tag{7}$$

The hydraulic diameter D_h and the molecular velocity υ_0 are taken as the characteristic length and velocity, respectively. Then, it is convenient to introduce the dimensionless spatial variables $x=\tilde{x}/D_h$, $y=\tilde{y}/D_h$, and $z=\tilde{z}/D_h$, the dimensionless cross section $A=\tilde{A}/D_h^2$, and perimeter $\Gamma=\tilde{\Gamma}/D_h$, as well as the dimensionless velocity $u=\tilde{u}/(\upsilon_0 X_P)$.

At this point it is important to note that under the assumption of $D_h \ll L$ the dimensionless pressure gradient is always much less than 1, i.e.

$$X_P = \frac{D_h}{P}\frac{dP}{d\tilde{z}} \simeq \frac{D_h}{L}\frac{\Delta P}{P} \ll 1, \tag{8}$$

independent of the magnitude of the pressure difference $\Delta P = P_1 - P_2$ between the two reservoirs.[8,28] This remark is easily explained by noting that even at large pressure differences, the ratio $\Delta P/P$ is at most of order of 1, while $D_h/L \ll 1$. Therefore, the quantity X_P will be used in the next section as a very small parameter to linearize the flow equations even at large pressure drops.

Closing this section, we focus on the specific four cross sections considered in the present work. Expressions for the quantities $D_h, \tilde{A}, A, \tilde{\Gamma}$ are specified in Table I, where D denotes the diameter of the circular cross section, H and W denote the height and the width of the orthogonal cross section, d denotes the side of the equilateral triangular cross section. Also, for the isosceles trapezoidal cross section B, b, and υ denote the large base, the small base, and the height, respectively, while ω is the acute angle $[\tan\omega = 2(\upsilon/B)/(1 - b/B)]$. It is seen that the circular and equilateral triangular

TABLE I. Expressions of D_h, $\tilde{A}$, A, $\tilde{\Gamma}$, and Γ for various cross sections.

Cross section	Hydraulic diameter D_h	Area $\tilde{A}$	Dimensionless area $A=\tilde{A}/D_h^2$	Perimeter $\tilde{\Gamma}$	Dimensionless perimeter $\Gamma=\tilde{\Gamma}/D_h$
Circular	D	$\pi D^2/4$	$\pi/4$	πD	π
Orthogonal	$2\dfrac{W\times H}{W+H}$	$W\times H$	$\dfrac{1}{4}\dfrac{H}{W}\left(1+\dfrac{W}{H}\right)^2$	$2(W+H)$	$\dfrac{H}{W}\left(1+\dfrac{W}{H}\right)^2$
Equilateral triangular	$d/\sqrt{3}$	$\sqrt{3}d^2/4$	$3\sqrt{3}/4$	$3d$	$3\sqrt{3}$
Isosceles trapezoidal	$\dfrac{2(B+b)\upsilon}{B+b+\dfrac{2\upsilon}{\sin\omega}}$	$\dfrac{B+b}{2}\upsilon$	$\dfrac{1}{8}\dfrac{\left(1+\dfrac{b}{B}+\dfrac{\upsilon}{B}\dfrac{2}{\sin\omega}\right)^2}{\left(1+\dfrac{b}{B}\right)\dfrac{\upsilon}{B}}$	$B+b+\dfrac{2\upsilon}{\sin\omega}$	$\dfrac{1}{2}\dfrac{\left(1+\dfrac{b}{B}+\dfrac{\upsilon}{B}\dfrac{2}{\sin\omega}\right)^2}{\left(1+\dfrac{b}{B}\right)\dfrac{\upsilon}{B}}$

cross sections are completely defined by specifying only the hydraulic diameter D_h, while for the orthogonal and isosceles trapezoidal cross sections additional parameters must be provided. In particular, for the orthogonal the ratio H/W and for the trapezoidal the ratios b/B and υ/B must be given. The geometric data for the specific four cross sections studied in the present work are provided in Table II of Sec. IV B.

III. THEORETICAL-COMPUTATIONAL APPROACH

The theoretical-computational approach is based on the Bhatnagar-Gross-Krook (BGK) kinetic equation subject to Maxwell boundary conditions with diffuse and specular boundary conditions. The problem is solved in a dimensionless form by the discrete velocity method yielding the unknown distribution function and the macroscopic velocity, which is integrated to deduce the flow rate. The analysis is general, and it may be applied to channels of any cross section. However, when a more detailed and comprehensive description for one of the specific cross sections under investigation is needed, it is accordingly provided. The computed quantities are dimensionalized by following a specific procedure in order to perform, later on (in Sec. V), a direct comparison with the experimental results using the experimental geometric and flow parameters.

A. Governing equations and boundary conditions

Since the problem is solved based on kinetic theory the main unknown is the distribution function which obeys a kinetic equation. It has been shown that fully developed isothermal pressure driven flows, as the ones described in Sec. II, can be simulated efficiently by the BGK model equation[29,30] given by

$$\xi_x\frac{\partial f}{\partial\tilde{x}}+\xi_y\frac{\partial f}{\partial\tilde{y}}=\frac{P}{\mu_0}(f^M-f), \tag{9}$$

where $\tilde{\boldsymbol{r}}=(\tilde{x},\tilde{y})$ is the position vector on a cross section, $\boldsymbol{\xi}=(\xi_x,\xi_y,\xi_z)$ is the molecular velocity vector, and $f=f(\tilde{\boldsymbol{r}},\boldsymbol{\xi})$ is the distribution function. Also the local Maxwellian f^M is given by

$$f^M=n\left(\frac{m}{2\pi kT_0}\right)^{3/2}\exp\left[-\frac{m(\xi-\tilde{u})^2}{2kT_0}\right], \tag{10}$$

with n denoting the local number density ($n=\rho/m$). By using the dimensionless quantities $\boldsymbol{r}=\tilde{\boldsymbol{r}}/D_h$, $\boldsymbol{c}=\boldsymbol{\xi}/\upsilon_0=(c_x,c_y,c_z)$, and $g=f/\upsilon_0^3$, we have the dimensionless BGK equation

$$c_x\frac{\partial g}{\partial x}+c_y\frac{\partial g}{\partial y}=\left(\frac{\sqrt{\pi}}{2}\frac{1}{\mathrm{Kn}}\right)(g^M-g), \tag{11}$$

where

$$g^M=\frac{n}{\pi^{3/2}\upsilon_0^3}\exp[-(c-u)^2]. \tag{12}$$

The validity of the BGK model to handle pressure driven flows has been, over the years, well verified. In particular, it has been shown that for flows between plates and through circular channels the discrepancy of the BGK model compared to other kinetic equations including the Boltzmann equation is less than 2%.[8] It is reasonable to expect that the validity of the BGK may be extended to other cross sections as well.

Even more, in the case of linear fully developed flows the distribution may be linearized according to

$$g=g^0[1+X_P(h(x,y,c)+z)], \tag{13}$$

where $h=h(x,y,c)$ is the linearized distribution and

$$g^0=n_0\exp(-c^2) \tag{14}$$

represents the absolute (or global) equilibrium at reference density n_0 and temperature T_0 ($P_0=n_0kT_0=\rho_0RT_0$). Substitut-

TABLE II. Geometric data for the four cross sections studied in the present work.

Cross section	Geometric data
Circular	$D_h=15.96$ mm
Orthogonal	$D_h=15.89$ mm, $H/W=1$
Equilateral triangular	$D_h=17.06$ mm
Isosceles trapezoidal	$D_h=16.48$ mm, $b/B=\upsilon/B=0.5$

ing expression (13) into Eq. (11) and expanding accordingly the Maxwellian (12) yield the linearized BGK equation,[12]

$$c_x\frac{\partial h}{\partial x}+c_y\frac{\partial h}{\partial y}+\delta h=2\delta c_z u-c_z, \tag{15}$$

where

$$u(x,y)=\frac{\tilde{u}}{v_0 X_P}=\frac{1}{\pi^{3/2}}\int_{-\infty}^{\infty}\int_{-\infty}^{\infty}\int_{-\infty}^{\infty}c_z h e^{-c^2}dc_x dc_y dc_z \tag{16}$$

is the macroscopic velocity in the z direction, deduced as it is seen by the first moment of h. Also,

$$\delta=\frac{\sqrt{\pi}}{2}\frac{1}{\mathrm{Kn}}=\frac{D_h P}{\mu_0 v_0} \tag{17}$$

is the so-called rarefaction parameter and it is proportional to the inverse Knudsen number ($\delta=0$ and $\delta\to\infty$ correspond to the free molecular and hydrodynamic limits, respectively).

At this point taking advantage of the two dimensionality of the flow is convenient to eliminate the c_z component of the molecular velocity vector by following the well known projection procedure.[12] First, the reduced distribution function

$$\Phi(x,y,c_x,c_y)=\frac{1}{\sqrt{\pi}}\int_{-\infty}^{\infty}c_z h(x,y,c_x,c_y,c_z)e^{-c_z^3}dc_z \tag{18}$$

is defined. Then, Eq. (15) is multiplied by $(1/\sqrt{\pi})c_z\exp(-c_z^2)$ and the resulting equation is integrated over all $-\infty<c_z<\infty$ to yield the reduced linearized BGK equation

$$c_x\frac{\partial\Phi}{\partial x}+c_y\frac{\partial\Phi}{\partial y}+\delta\Phi=\delta u-\frac{1}{2}. \tag{19}$$

The macroscopic velocity in terms of Φ is given as

$$u(x,y)=\frac{1}{\pi}\int_{-\infty}^{\infty}\int_{-\infty}^{\infty}\Phi\ \exp[-c_x^2-c_y^2]dc_x dc_y. \tag{20}$$

It is seen that the deduced Eq. (19) for the unknown distribution $\Phi=\Phi(x,y,c_x,c_y)$ does not contain the independent variable c_z. The reduction in the number of independent variables by 1 reduces significantly the computational effort associated with the implemented discrete velocity scheme discussed in the next section.

The gas-wall interaction is modeled by the Maxwell diffuse-specular reflection condition.[7] At the boundaries we have

$$f^+=\alpha f_w^M+(1-\alpha)f^-, \tag{21}$$

where f^+ and f^- are the distributions representing particles departing and arriving at the wall, respectively, while f_w^M is the Maxwellian defined by the wall temperature. The parameter $\alpha\in[0,1]$ is the so-called tangential momentum accommodation coefficient and denotes the portion of the particles reflecting diffusively from the wall. Applying the above described procedure (nondimensionalization, linearization, projection) the boundary condition for the reduced distribution becomes[15,16]

$$\Phi^+=(1-\alpha)\Phi^-, \tag{22}$$

where again the superscripts $(+)$ and $(-)$ denote particles departing and arriving at the wall, respectively.

The linear integrodifferential equation (19), supplemented by the corresponding integral expression (20) and subject to the boundary condition (22), is solved numerically. The implemented numerical scheme has been described, in detail, for channels with circular, rectangular, and triangular cross sections in a series of previous works.[12,15,16,31] For the trapezoidal cross section we follow the procedure introduced in Ref. 16, by implementing a corresponding boundary fitted lattice. In all cases, the kinetic equation is discretized in the molecular velocity space by the discrete velocity method and in the physical space by typical finite difference schemes. Then, the discretized equations are solved in an iterative manner.

B. Computed quantities

The kinetic solution depends on three dimensionless parameters, namely, the reference rarefaction parameter δ, the area of the cross section A, and the accommodation coefficient α. Based on the kinetic solution, which is valid in the whole range of the Knudsen number, from the free molecular, through the transition and slip regimes up to the hydrodynamic limit, several overall macroscopic quantities of practical interest may be deduced.

Here, we are interested in the mass flow rate, which may be obtained by integrating the velocity distribution across the cross section of the channel as

$$Q_m=\int_{\tilde{A}}\rho(\tilde{z})\tilde{u}(\tilde{x},\tilde{y})d\tilde{A}. \tag{23}$$

The double integral at the right hand side of Eq. (23) is nondimensionalized, and by using the equation of state ($\rho=2P/v_0^2$) as well as the fact that the mass density depends only on $\tilde{z}$, it is deduced that

$$Q_m=G\frac{\tilde{A}PX_P}{v_0}=G\frac{\tilde{A}D_h}{v_0}\frac{dP}{d\tilde{z}}, \tag{24}$$

where

$$G=\frac{2}{A}\iint_A u dA. \tag{25}$$

Traditionally, the quantity G is referred to the literature as the reduced (or dimensionless) flow rate[7,8] and it is obtained by the kinetic solution. Once the kinetic problem is solved, G is readily deduced from the double integral in Eq. (25).

In the case of a specific application the hydraulic diameter D_h, the area $\tilde{A}$ and the perimeter $\tilde{\Gamma}$ of the cross section along with the length L of the channel are defined. Based on these geometric data the dimensionless quantities A and Γ are easily estimated. In addition, the upstream and downstream pressures P_1 and P_2, respectively, as well as the reference temperature T_0 are provided. Also, the type of the gas and its characteristic molecular velocity v_0 are known. Then, the rar-

efaction parameter δ can be estimated, by Eq. (17), for any pressure $P \in [P_1, P_2]$. When the pressure difference is small it is adequate to define an average rarefaction parameter $\delta_0 = (\delta_1 + \delta_2)/2$, where δ_1 and δ_2 correspond to pressures P_1 and P_2, respectively, and based on the kinetic solver to compute the corresponding dimensionless flow rate $G(\delta_0)$. In this case the mass flow rate can be estimated by the expression[8,15,16]

$$Q_m = G(\delta_0)\frac{\tilde{A}D_h}{\upsilon_0}\frac{P_1 - P_2}{L}. \tag{26}$$

When the pressure difference is large then the above expression is slightly modified. In particular, it is supplemented by a well known procedure, which is based on the mass conservation principle. In the case of large pressure drops the mass flow rate is estimated by[8,15,16]

$$Q_m = G^*\frac{\tilde{A}D_h}{\upsilon_0}\frac{P_1 - P_2}{L}, \tag{27}$$

where now G^* is obtained by integrating over all $\delta \in [\delta_1, \delta_2]$, i.e.,

$$G^* = \frac{1}{\delta_1 - \delta_2}\int_{\delta_2}^{\delta_1} G(\delta)d\delta. \tag{28}$$

It is easily seen that in the case of small pressure drops, $G^* = G(\delta_0)$.

Another quantity of practical interest is the conductance C, expressed as[1]

$$C = \frac{Q_m}{M}\frac{RT_0}{\Delta P}, \tag{29}$$

with M denoting the molar mass of the gas.

At this point, it is useful to define the reference Knudsen, Reynolds, and Mach numbers of the flow in terms of the reference pressure $P_0 = (P_1 + P_2)/2$ and the corresponding reference rarefaction parameter δ_0. Based on Eqs. (3)–(5) it is easily reduced that

$$\mathrm{Kn}_0 = \frac{\sqrt{\pi}}{2}\frac{1}{\delta_0} = \frac{\sqrt{\pi}}{2}\frac{\mu_0\upsilon_0}{D_h P_0}, \tag{30}$$

$$\mathrm{Re}_0 = \frac{\rho_0 \tilde{U}_0 D_h}{\mu_0} = 2\delta_0 U_0 \frac{D_h}{L}\frac{P_1 - P_2}{P_0}, \tag{31}$$

and

$$\mathrm{Ma}_0 = \frac{\tilde{U}_0}{c_0} = \sqrt{\frac{2}{\gamma}}U_0\frac{D_h}{L}\frac{P_1 - P_2}{P_0}. \tag{32}$$

In Eqs. (38) and (39) the quantity

$$U_0 = \frac{\tilde{U}_0}{\upsilon_0 X_P} = \frac{1}{A}\iint_A u dA \tag{33}$$

is the dimensionless mean velocity and it is obtained from the kinetic solution, while all other quantities have been earlier defined. Results of these reference numbers are reported in Sec. V for the specific geometric and flow parameters, which are used in the experimental work and provide a more complete understanding and a better insight in the flow characteristics.

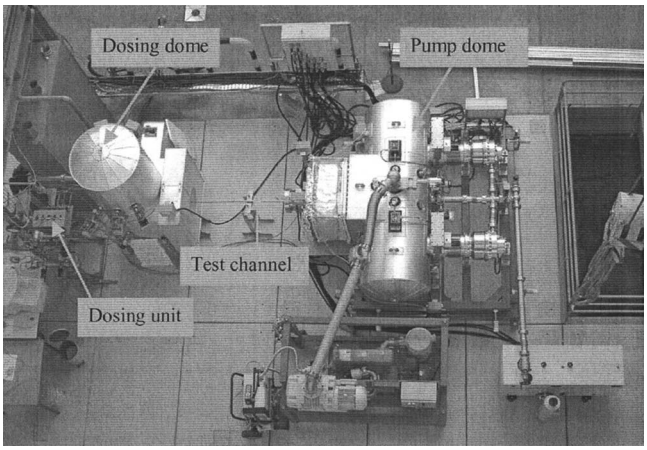

FIG. 1. Overview of the TRANSFLOW test rig.

Finally, it is noted that following the estimation of the mass flow rate Q_m, it is possible to compute the pressure distribution along the channel. Equation (24) is written in the form

$$\frac{dP}{dz} = \frac{Q_m \upsilon_0 L}{G(\delta)\tilde{A}D_h}, \tag{34}$$

and then the above first order ordinary differential equation, with initial condition $P(0) = P_1$, may be solved numerically applying any typical integration scheme. For example, dividing the distance $0 \leqslant z \leqslant 1$ into N intervals of length Δz and applying to Eq. (34) a first order Euler scheme yields the finite difference expression

$$P(z_i) = P(z_{i-1}) + \frac{Q_m \upsilon_0 L}{\tilde{A}D_h}\frac{\Delta z}{G(\delta_{i-1})}, \quad i = 1,2,\ldots,N, \tag{35}$$

which produces the pressure distribution along the channel. Then, provided that the discretization is dense enough and that the mass flow rate Q_m has been estimated correctly, the downstream pressure $P(1) = P_2$ at $z = 1$ is recovered. It is obvious that this analysis can be also used in cases where the downstream pressure is unknown provided that the mass flow rate is given.

IV. EXPERIMENTAL APPROACH

A. Basic design of the TRANSFLOW test rig

The basic principle of the (see Fig. 1) transitional flow range experiments (TRANSFLOW) test rig is the measurement of the conductance of different channels in the transitional and near transitional flow regime at isothermal conditions. TRANSFLOW is based on the direct dynamic approach, where a constant flow Q_m is adjusted and the pressure difference ΔP is measured. Then, the conductance is estimated using Eq. (29). The constant flow into the test rig is provided by a dosing unit. The temperature and pressure of

the injected gas can be measured in the dosing dome, which is directly connected to the dosing unit. The effective cross section of the dome is very big compared to the cross section of the duct so as to make the pressure differences between these two elements as small as possible. The test channel is following the dosing dome in flow direction, and on the downstream end it is connected with the pump dome. The pump dome serves to measure temperatures and pressures at the outlet side of the test channel, and is also equipped with the turbomolecular pumps which are further connected to the forepumps, to maintain the vacuum conditions inside the system. The whole facility is designed for fundamental laboratory research, but sufficiently large to investigate 1:1 scale big vacuum components (valves, bellows, etc.) with a connection diameter up to 600 mm diameter. To be most versatile, the pump dome is installed in two separate frames and can be moved relative to the dosing dome so that the connection element must not necessarily be straight.

The dosing unit consists of five thermal mass flow controllers in parallel. The flow ranges of the different mass flow controllers are chosen depending on the estimated flows for the tests. Mass flow controller with the maximum ranges of 1, 10, 100, 1000, and 10 000 SCCM (SCCM denotes cubic centimeter per minute at STP) (always nitrogen equivalent) are installed. The summarized flow range is therefore between 0.02 and 11 111 SCCM. All used mass flow controllers were individually calibrated for nitrogen and helium. During commissioning of the facility, mass flow measurements based on orifices under choked flow conditions were used for comparison.

The dosing dome provides an isothermal and isotropic flow at a constant pressure difference through the test channel. It consists of two sections: The upper section is identical with a PNEUROP dome.[32] The inlet pipe is bent to the inner top of the dosing dome to reduce streaming effects in the gas flow. The lower part is a cylinder with the same inner diameter as the upper part. On the gas outlet side the dosing dome features a square shaped flange with an inner length of 600 mm. The flange holds the test channel directly or via an adapter flange, if the cross section of the test channel is smaller.

The pump dome connects the different test channels and the vacuum pumps. It consists of a horizontally orientated cylinder with a square shaped flange in the middle. The square shaped flange has the same dimensions as the flange on the dosing dome (600 mm inner length). The flange holds a large compensator, which has been designed for length and small angular compensation. Between the compensator and the test channel different adapter flanges can be installed.

There are three gauges and one Bayard–Alpert gauge mounted on the dosing and the pump dome, respectively. The capacitance gauges are cascaded with a full scale of 1000, 10, and 1 Torr in the case of the dosing dome and 1000, 10, and 0.1 Torr in the case of the pump dome. By cascading with overlapping ranges, the resulting experimental error in pressure measurement, which is constant for the full range, can be significantly reduced. The gauges have been calibrated for nitrogen. The two Bayard–Alpert gauges have a typical measurement range between 10^{-2} and 10^{-10} mbar. One is installed in the upper part of the dosing dome, the other in the middle of the pumping dome. Both gauges are calibrated for nitrogen and helium.

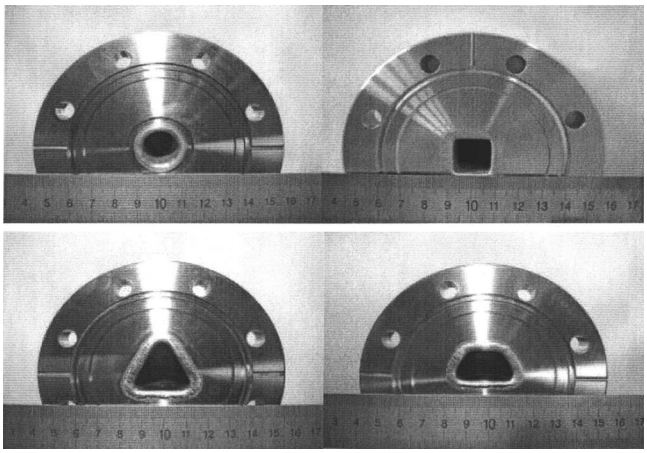

FIG. 2. Circular, square, equilateral triangular, and isosceles trapezoidal cross sections.

The two platinum resistances based temperature sensors of the domes are positioned so that they measure the temperature in the middle of the gas stream. One is installed in the lower part of the dosing dome in horizontal direction and the second one on the top of the square shaped part of the pump dome in vertical direction.

B. Channel geometry and characteristics

Four stainless steel test channels with different cross sections were used for the experiments in TRANSFLOW, namely, a circular, square shaped, equilateral triangular, and an isosceles trapezoidal cross section (see Fig. 2). All four channels had a length equal to $L=1277$ mm and a hydraulic diameter of approximately 16 mm so that a length to diameter ratio of 80 is reached. Due to the manufacturing uncertainties, the hydraulic diameters differ from the theoretical one and were determined by measurements. The resulting values are shown in Table II. The inner surface of the channels was of standard clean technical quality without special treatment. On both ends flanges DN 63 CF are welded, which are used for the installation of the test channels between the adapter flanges of the dosing and the pump dome.

C. Measurement procedure and data evaluation

The experiments with all channels have been performed at constant gas flows in the full range of different flow regimes. The flow rate of 0.02 SCCM is the lowest achievable at good reproducibility. For the given channels, the highest flow rate chosen is 110 SCCM, which is sufficient to have several measurement points in the viscous flow regime. The test gas in all experiments is nitrogen at ambient temperature conditions.

TABLE III. Typical contributions to the overall measurement uncertainty.

Uncertainty	For flow measurement	For pressure measurement
Quantitative instrumentcalibration	1.5%–2.5% of the measured value	0.5% of the measured value (capacitance gauges); 5% (Bayard–Alpert gauges)
Relative standard deviation of the measurement values in the evaluated time interval (95% confidence interval)	<0.1%	<0.1% (capacitance gauges); negligible (Bayard–Alpert gauges)
Offset drift within one week (zeroed out each week)	Last of the four significant digits	Last of the five significant digits
Maximum error of multimeter (voltage measurement)	…	0.005%

During a measurement, the flow rate, the temperature, and the pressure in the dosing dome and in the pumping dome are recorded, stored by the data acquisition system (at a frequency of 2 values/min) and finally corrected by use of calibration tables. The final data are taken after an equilibration period of several hours; typically, an ensemble of 50–100 measurement values is evaluated. For the pressure measurement, the effect of thermal transpiration between the temperature of the gauge head (maintained at the constant temperature of 313 K) and the gas is being considered.[33] In a final evaluation step, the thus obtained pressures in the domes are further corrected for the pressure difference between the channel inlet or outlet and the corresponding dome volume. This is done by use of a semiempirical code to assess conductance in networks.[34] These corrections are in the order of well below 0.5% of the measured ΔP.

The uncertainties of the measured values are given by a combination of the individual uncertainties of the sensors and data acquisition uncertainties. Table III summarizes the different contributions to the overall experimental uncertainty. It becomes obvious that the uncertainties associated with the calibration of the instruments (done against a secondary standard) in terms of absolute measurement values are clearly dominating the overall experimental error.

In the following section, the experimental values are compared with the calculation results. On top of the uncertainties (about 5%), associated with the measurements described above, the comparison results are strongly influenced by the absolute value for the hydraulic diameter D_h. The conductance, for example, depends on D_h by the power of 3 (molecular flow) up to 4 (viscous flow). The hydraulic diameters, given in Table II, have been derived from an integral volumetric measurement, which delivers the cross section at a very high accuracy (in the order of 0.01%) and from the perimeter, as it is estimated from the shop drawings under the assumption of a mathematically perfect shape (cycle, orthogonal, etc.). However, this latter assumption, due to the rounded edges of the channels, introduces an error to the estimation of the hydraulic diameters. It is noted that it was possible to measure the exact perimeter. In any case according to our calculations the introduced maximum uncertainty is about 4%. In future work, a more accurate determination of the hydraulic diameter will be attempted by using nondestructive examination techniques to estimate local cross sections and their corresponding profiles across the channel length.

V. RESULTS AND DISCUSSION

Computational and experimental results are presented for all four cross sections under consideration. The accuracy of the numerical results has been tested in several ways. For small values of δ we need a large number of discrete velocities, while the physical grid may be coarse. For large values of δ, the required number of discrete velocities may be reduced but dense physical grids are important to achieve good accuracy. Depending on the value of δ and the geometry, the discretization has been progressively refined to ensure grid independent results up to at least three significant figures within ± 1 to the last one. In addition, the computational results always recover the well known solutions at the free molecular and hydrodynamic limits. The accuracy of the experimental results has been discussed, in detail, in Sec. IV C.

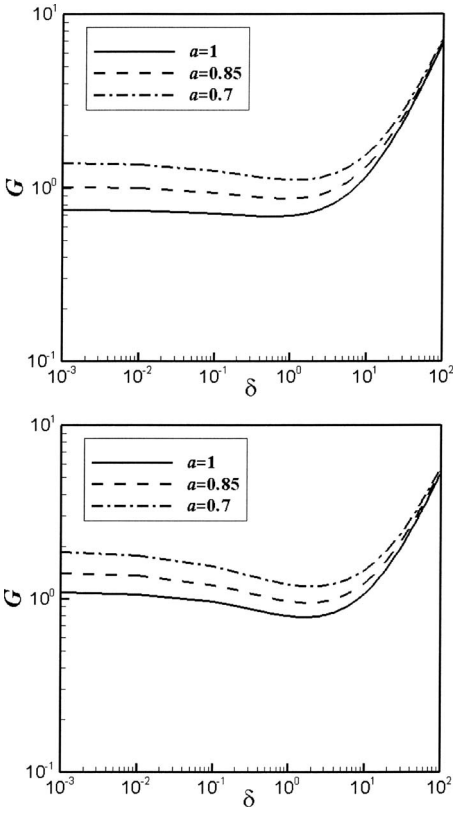

FIG. 3. Dimensionless flow rates in long channels of circular (top) and orthogonal with $H/W=0.1$ (bottom) cross sections for various values of α.

TABLE IV. Computed dimensionless flow rates G in long channels of various cross sections in terms of δ, with $\alpha=1$.

		Orthogonal			
δ	Circular	$H/W=1$	$H/W=0.1$	Equilateral triangular	Isosceles trapezoidal $b/B=v/B=0.5$
0	0.752	0.839	1.09	0.930	0.879
0.01	0.743	0.828	1.06	0.916	0.879
0.1	0.715	0.793	0.961	0.872	0.827
0.5	0.689	0.762	0.838	0.831	0.790
1	0.693	0.768	0.796	0.833	0.793
1.5	0.709	0.786	0.785	0.851	0.809
2	0.729	0.809	0.786	0.874	0.831
3	0.776	0.864	0.804	0.931	0.885
4	0.829	0.924	0.833	0.994	0.943
5	0.883	0.987	0.867	1.06	1.00
7	0.997	1.117	0.944	1.19	1.13
10	1.17	1.32	1.07	1.41	1.33
20	1.78	2.00	1.51	2.14	2.02
30	2.40	2.70	1.98	2.87	2.71
40	3.02	3.40	2.44	3.61	3.41
50	3.64	4.10	2.91	4.36	4.10
60	4.27	4.80	3.38	5.10	4.8
70	4.89	5.50	3.85	5.84	5.48
80	5.51	6.20	4.32	6.58	6.07
90	6.14	6.90	4.79	7.31	6.86
100	6.76	7.61	5.26	8.04	7.55

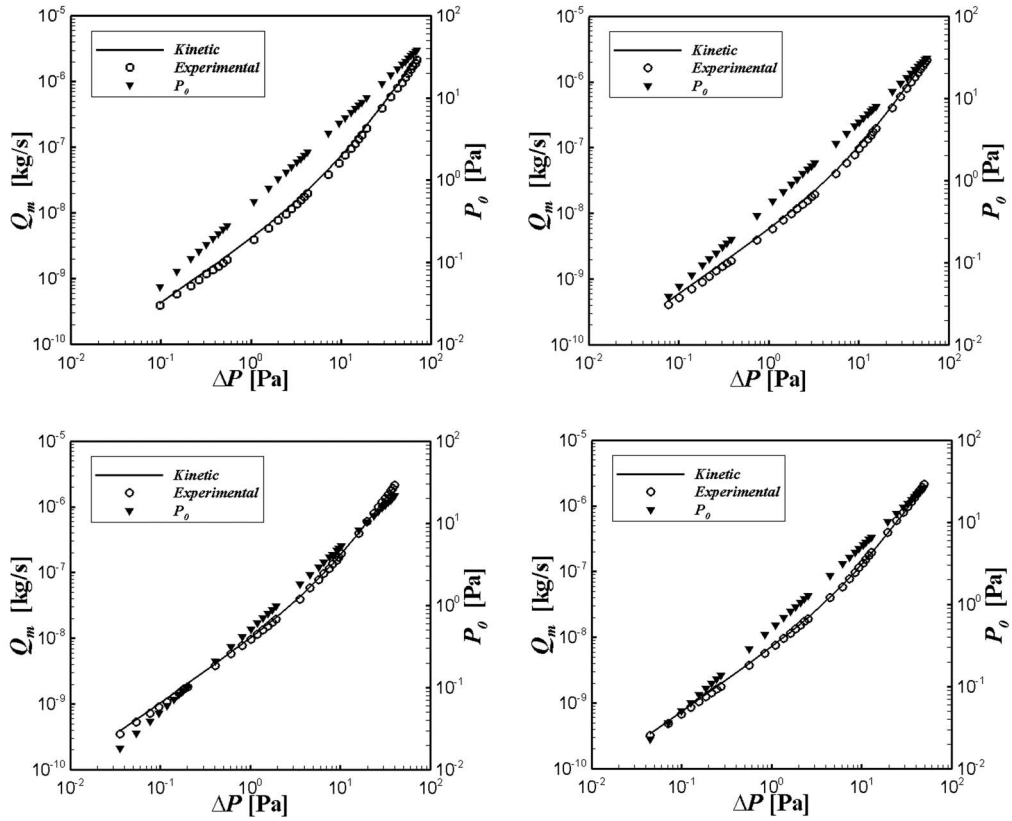

FIG. 4. Experimental and computational mass flow rates in terms of ΔP and P_0 for channels of various cross sections (top left: circular; top right: square; bottom left: equilateral triangular; bottom right: isosceles trapezoidal with $b/B=v/B=0.5$).

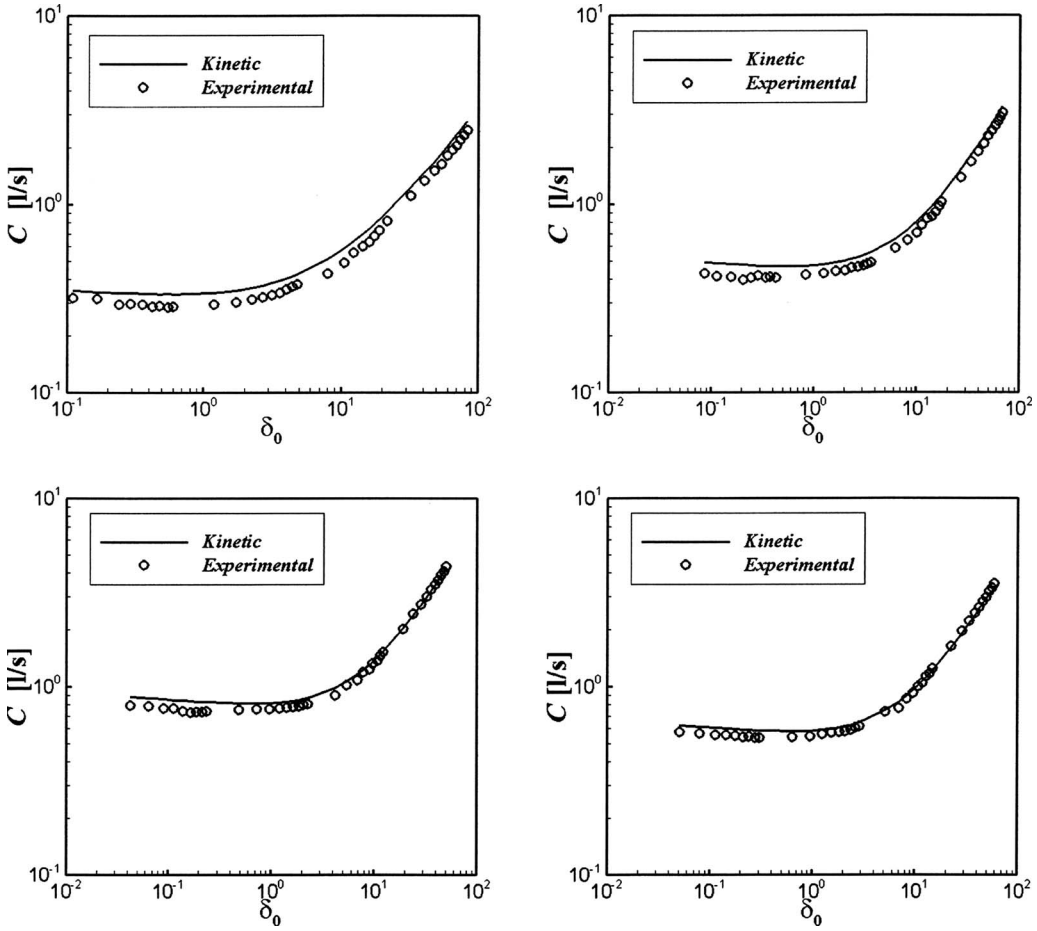

FIG. 5. Experimental and computational conductance in terms of the rarefaction parameter δ for channels of various cross sections (top left: circular; top right: square; bottom left: equilateral triangular; bottom right: isosceles trapezoidal with $b/B=v/B=0.5$).

The dimensionless flow rate G is shown in Table IV in terms of the rarefaction parameter δ for channels with circular, orthogonal ($H/W=1$ and 0.1), equilateral triangular, and isosceles trapezoidal ($b/B=v/B=0.5$) cross sections. The accommodation coefficient has been taken $\alpha=1$. It is seen that the qualitative behavior of G in terms of δ is similar for all cross sections, although qualitatively there are differences. Note that the Knudsen minimum is always about 1 but occurs at different δ for each cross section. In some cases the Knudsen minimum is deep (orthogonal channel with $H/W=1$), while in others is shallow (e.g., circular channel). Also, the limiting values of G at $\delta=0$ are different, while as we are getting into the slip regime ($\delta>10$), G in all cases becomes proportional to δ but the proportionality constant is different for each cross section. The results of Table IV, regarding the circular, orthogonal, and triangular cross sections, have been reported before,[8,12,16] while the results for the trapezoidal one are reported for first time in the literature. In addition, the results of Table IV are all based on the same characteristic length, which is the hydraulic diameter D_h, while in previous works various characteristic lengths have been implemented depending on the geometry, i.e., the radius R for circular channels in Ref. 8 and the height H for orthogonal channels in Ref. 12. The present results are in excellent agreement with the corresponding ones in Refs. 8 and 12 taking into account the different characteristic lengths. In particular, if we denote the dimensionless flow rates for a circular channel in Ref. 8 and for a rectangular channel in Ref. 12 by G_R and G_H, respectively, then these quantities are related to the corresponding present ones according to

$$G=\tfrac{1}{2}G_R\left(\tfrac{1}{2}\delta\right) \tag{36}$$

and

$$G=\frac{H}{D_h}G_H\left(\frac{H}{D_h}\delta\right), \tag{37}$$

where $H/D_h=(1+H/W)/2$.

The dependency of the dimensionless flow rate with respect to the tangential momentum accommodation coefficient α is shown in Fig. 3, where results of G are shown for channels with circular and orthogonal cross sections with $\alpha=1$, 0.85, and 0.70. It is seen that as α is decreased (i.e., less diffuse reflection), G is increased. This is expected since as the interaction between the molecules and the wall becomes more specular the friction factor at the wall is decreased. It is also seen that the effect of α on G is more dominant in the free molecular regime (small values of δ), it decays gradu-

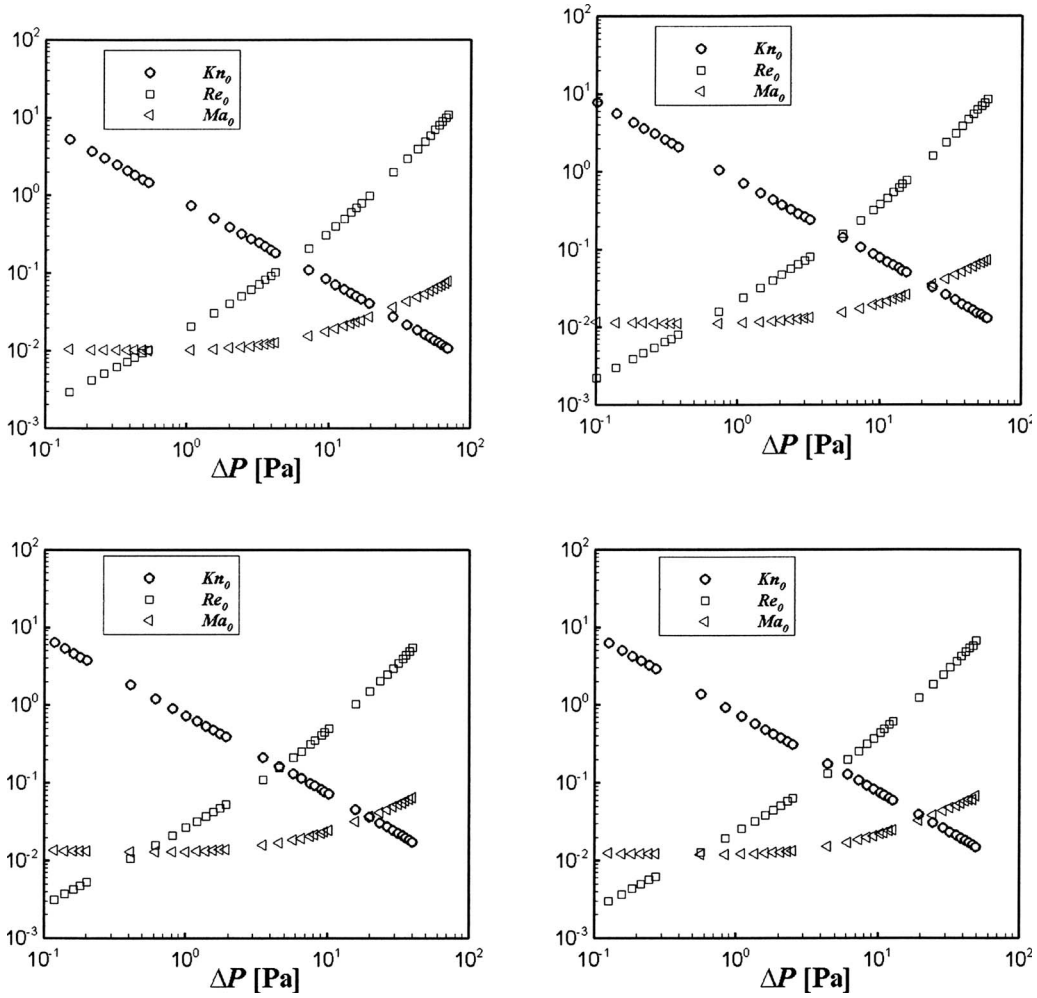

FIG. 6. Reference Knudsen, Mach, and Reynolds numbers in terms of pressure difference ΔP for channels of various cross sections (top left: circular; top right: square; bottom left: equilateral triangular; bottom right: isosceles trapezoidal with $b/B=v/B=0.5$).

ally as δ is increased, and finally at the hydrodynamic limit there no effect at all. This behavior is typical for any cross section.

We continue now, in Fig. 4, with the comparison between computational and available experimental results for each of the four cross sections under consideration. Each experiment is characterized by a pressure difference $\Delta P=P_1-P_2$ and by a reference pressure $P_0=(P_1+P_2)/2$. Both quantities are indicated in Fig. 4. The pressure difference ΔP is shown on the horizontal axis and the reference pressure P_0 on the right vertical axis. For each pair $(P_0,\Delta P)$ the corresponding computed (solid line) and measured (cycles) mass flow rates are shown. The computed quantities have been obtained by dimensionalizing the tabulated results of Table IV according to the procedure discussed in Sec. III B. For all four cross sections the agreement between computational and experimental results is considered as very good in the whole range of $(P_0,\Delta P)$. The relative errors defined as $|(Q_m^{\mathrm{comp}}-Q_m^{\mathrm{exper}})/Q_m^{\mathrm{comp}}|$ for all cross sections vary from less than 1% up to about 10%, while the average error is estimated around 5%. These discrepancies are attributed to errors in measurements (maximum about 5%), in the estimation of hydraulic diameter (maximum about 4%) and also in modeling due to the implementation of the BGK, instead of the Boltzmann equation (about 2%). These introduced uncertainties justify the observed differences between experimental and computed results.

The corresponding computational and experimental results for the conductance C in l/s are presented in terms of the rarefaction parameter δ in Fig. 5. It is seen that again the agreement is very good. In general, the conductance is almost constant at rarefied atmospheres up to some value of δ, and then as we are getting into the slip and viscous regimes it is increased proportionally to δ. Both computed and measured results confirm the existence of the Knudsen minimum in all cross sections.

In Fig. 6, for each cross section and for each experimental pair $(P_0,\Delta P)$ the reference Kn_0, Re_0, and Ma_0, estimated by Eqs. (30)–(32), respectively, are shown. The Knudsen number is reduced linearly in a log-log scale as ΔP is increased and varies between 10^{-2} and 10^{2}. Therefore, it is seen that the presented results cover all four regimes from rough up to high vacuum. The Reynolds number is increased as ΔP is increased but in all cases remains small and varies from 10^{-3}

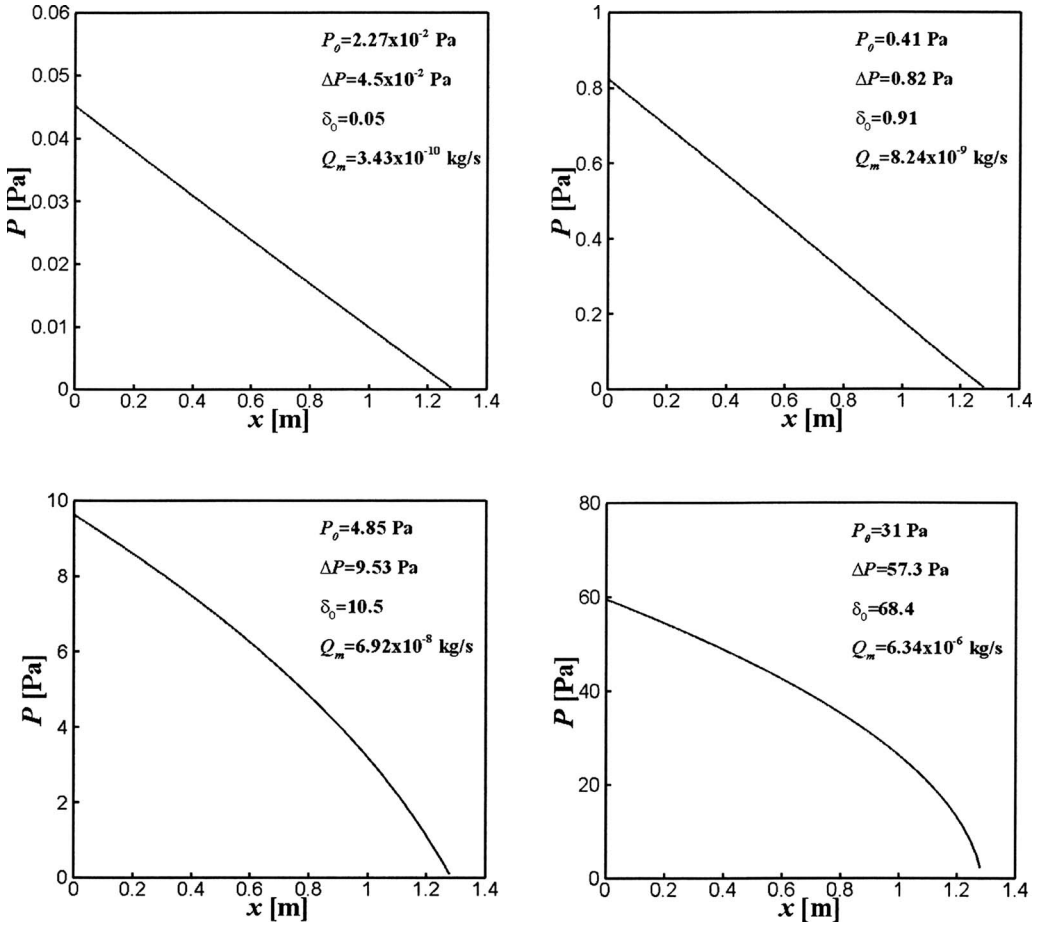

FIG. 7. Typical pressure distributions along the channel (top left: isosceles trapezoidal with $b/B=v/B=0.5$; top right: equilateral triangular; bottom left: circular; bottom right: square).

and 10. It is reasonable to expect that in all cases the flow is laminar even when it is well inside the viscous (continuum) regime. Finally, as expected the Mach number is very small ranging between 10^{-2} and 10^{-1}. Actually, for a wide range of ΔP remains constant and then as ΔP increases the Mach number is moderately increased. All this information related to the flow properties and characteristics is particularly useful.

Finally, in Fig. 7, pressure drop distributions along the channels are presented for four typical cases. Each of the four presented pressure distributions correspond to a different cross section and to a different pair of data $(P_0, \Delta P)$. Also, each pair of data corresponds to one of the four flow regimes. In particular, the presented pressure drop distributions for the trapezoidal, triangular, circular, and square channels correspond to the free molecular, transition, slip, and viscous regimes, respectively. Therefore, a representative picture for the pressure distribution in each flow regime may be obtained. It is seen that when the flow is in the free molecular regime ($\delta=0.05$) and also in the middle of the transition regime ($\delta=0.91$) the pressure distribution is linear, while as the flow is just getting into the slip regime ($\delta=10.5$) and also inside the viscous regime ($\delta=68.4$), the pressure distributions become parabolic. This behavior of the pressure distribution along the channel in the slip and viscous regimes has been also observed in Refs. 24 and 35.

VI. CONCLUDING REMARKS

A computational and experimental study has been performed for the investigation of fully developed gas flows through channels of circular, orthogonal, triangular, and trapezoidal cross sections in the whole range of the Knudsen number. The theoretical-computational approach is based on the BGK kinetic theory subject to Maxwell diffuse-specular boundary conditions. The experimental work has been performed at the vacuum test facility TRANSFLOW at FZK. The computed and measured flow rates and conductance are in all cases in very good agreement. The discrepancies are within 10%. In addition, the reference Knudsen, Reynolds, and Mach numbers characterizing the flow in all experimental runs have been estimated. Also, the pressure distribution along the channel has been presented for several representative cases.

It may be concluded that kinetic theory is probably the only theoretical approach to yield accurate results in a unified manner for any type of vacuum conditions from rough all the way down to ultrahigh vacuum. In addition, it has

been verified that the developed and applied experimental methodology and procedure in the TRANSFLOW facility are valid and accurate and may be implemented to more complex flow configurations.

ACKNOWLEDGMENTS

This work has been supported by the European Communities under the contract of Association EURATOM/Forschungszentrum Karlsruhe and EURATOM/Hellenic Republic. The work of V. Hauer and C. Day has been carried out within the framework of the European Fusion Development Agreement. The views and opinions expressed herein do not necessarily reflect those of the European Commission.

[1]W. Umrath, *Fundamentals of Vacuum Technology* (Leybold, Cologne, 1998).
[2]M. Gad-el Hak, *The MEMS Handbook* (CRC, Boca Raton, FL, 2002).
[3]J. H. Ferziger and H. G. Kaper, *Mathematical Theory of Transport Processes in Gases* (North-Holland, Amsterdam, 1972).
[4]G. A. Bird, *Molecular Gas Dynamics and the Direct Simulation of Gas Flows* (Oxford University Press, Oxford, 1994).
[5]Y. Sone, *Kinetic Theory and Fluid Mechanics* (Birkhauser, Boston, 2002).
[6]J. M. Reese, M. A. Gallis, and D. A. Lockerby, Philos. Trans. R. Soc. London, Ser. A **361**, 2967 (2003).
[7]C. Cercignani, *The Boltzmann Equation and its Application* (Springer-Verlag, New York, 1988).
[8]F. Sharipov and V. Seleznev, J. Phys. Chem. Ref. Data **27**, 657 (1998).
[9]Y. Sone and M. Hasegawa, J. Vac. Soc. Jpn. **30**, 425 (1987).
[10]M. Hasegawa and Y. Sone, J. Vac. Soc. Jpn. **3**, 416 (1988).
[11]K. Aoki, in *Rarefied Gas Dynamics*, edited by E. P. Muntz, D. P. Weaver, and D. H. Campbell (AIAA, Washington DC, 1989), Vol. 118, pp. 297–322.
[12]F. Sharipov, J. Vac. Sci. Technol. A **17**, 3062 (1999).
[13]D. Valougeorgis and S. Naris, SIAM J. Sci. Comput. (USA) **25**, 534 (2003).
[14]I. Graur and F. Sharipov, Eur. J. Mech. B/Fluids **27**, 335 (2008).
[15]G. Breyiannis, S. Varoutis, and D. Valougeorgis, Eur. J. Mech. B/Fluids **27**, 609 (2008).
[16]S. Naris and D. Valougeorgis, Eur. J. Mech. B/Fluids **27**, 810 (2008).
[17]A. K. Streekanth, Proceedings of the Sixth International Symposium on Rarefied Gas Dynamics on Slip Flow Through Long Circular Tubes, edited by L. Trilling and H. Y. Wachman (Academic, San Diego, CA, 1969), pp. 667–680.
[18]E. Suetin, B. T. Porodnov, V. G. Chernjak, and S. F. Borisov, J. Fluid Mech. **60**, 581 (1973).
[19]B. T. Porodnov, P. E. Suetin, S. F. Borisov, and V. D. Akinshin, J. Fluid Mech. **64**, 417 (1974).
[20]S. Tison, Vacuum **44**, 1171 (1993).
[21]L. Marino, Experiments on Rarefied Gas Flows Through Tubes, Microfluid. Nanofluid, DOI: 10.1007/s1040-008-0311-7 (Springer, Berlin/Heidelberg, 2008).
[22]Y. Zohar, S. Y. Kwan Lee, W. Y. Lee, L. Jiang, and P. Tong, J. Fluid Mech. **472**, 125 (2002).
[23]S. Colin, P. Lalonde, and R. Caen, Heat Transfer Eng. **25**, 23 (2004).
[24]J. Jang and T. Wereley, Microfluid. Nanofluid. **1**, 41 (2004).
[25]S. Colin, Microfluid. Nanofluid. **1**, 268 (2005).
[26]T. Ewart, P. Perrier, I. A. Graur, and J. G. Meolans, Exp. Fluids **41**, 487 (2006).
[27]T. Ewart, P. Perrier, I. A. Graur, and J. G. Meolans, J. Fluid Mech. **584**, 337 (2007).
[28]F. Sharipov and V. D. Seleznev, J. Vac. Sci. Technol. A **12**, 2933 (1994).
[29]P. L. Bhatankar, E. P. Gross, and M. Krook, Phys. Rev. **94**, 511 (1954).
[30]P. Welander, Ark. Fys. **7**, 507 (1954).
[31]S. Naris, D. Valougeorgis, F. Sharipov, and D. Kalempa, Superlattices Microstruct. **35**, 629 (2004).
[32]*Vacuum Pump Acceptance Specifications* (British Compressed Air Society, London, 1989).
[33]T. Takaishi and Y. Sensui, Trans. Faraday Soc. **59**, 2503 (1963).
[34]Chr. Day, V. Hauer, G. Class, D. Valougeorgis, and M. Wykes, Development of a simulation code for ITER vacuum flows, IAEA Fusion Energy Conference, Chengdu, China, October 2006 (unpublished), Paper IT/P2-12, published on web http://www-naweb.iaea.org/napc/physics/FEC/FEC2006/papers/it_p2-12.pdf.
[35]C. Shen, J. Fan, and C. Xie, J. Comput. Phys. **189**, 512 (2003).